Mimulus Keeps the Score: Investigating Transgenerational Plasticity in Response to Temperature in *Mimulus laciniatus*

Charlie R. Kortleven

ABSTRACT

Plants can respond to environments experienced by previous generations through transgenerational plasticity (TGP), whereby parental environmental effects alter phenotypic and genotypic expression in progeny. Theory predicts that TGP can evolve when the environment is temporally autocorrelated, when there is genetic variation in the norm of reaction, and when the cost of responding is low. Although previous research provided some insight into how TGP is induced and persists, the distinct genetic components that mediate TGP and that contribute to its evolution are less understood. *Minulus laciniatus* offers a tractable study system for investigating TGP and its evolution across an elevational and geographic gradient. To characterize the genetic basis of natural variation for both within-generation plasticity (WGP), TGP, and phenotypic variation to temperature, we employed a Multiparent Advanced Generation Inter-Cross (MAGIC) scheme from six parental inbred lines. Using recombinant inbred lines, we simulated diurnal temperature patterns from the warmest (H) and coldest (C) environments experienced by natural populations in a full factorial design to map quantitative trait loci (QTLs). To identify candidate genes mediating TGP within these QTLs, we performed RNA-Seq of the parental lines to find genes differentially expressed between C x C and H x C treatments. Preliminary mapping results suggest an absence of QTL for TGP, but indicate floral tube length, flower anthocyanin, and corolla width responses to cold (C x C) have a rather simple genetic basis, and temperature-dependent WGP. Transcriptomic results suggest that transgenerational effects tend to globally downregulate gene expression in offspring, with population-specific magnitude.

KEYWORDS

Transgenerational Plasticity (TGP), Within-generation Plasticity (WGP), Phenotypic variation, Quantitative trait loci (QTL), Multi-parent advanced generation intercross (MAGIC)

INTRODUCTION

In California, as atmospheric CO2 concentrations continue to rise, mean temperatures are projected to increase and precipitation rates decrease (Intergovernmental Panel on Climate Change (IPCC) 2023), resulting in changes that require organisms to rapidly acclimate to changing abiotic stressors. The capacity of one genotype to produce multiple phenotypes in response to varying environmental conditions (Schlichting 2024) is a taxonomically widespread phenomenon and can provide a means for organisms to cope with novel environments. Many studies have documented genotype x environment interactions, and the adaptive value of an organism's ability to integrate environmental and developmental cues into its regulatory machinery (Nicotra et al. 2010). Yet, it is uncertain whether within-generation plasticity (WGP) alone will allow plants to keep pace with the rate at which the climate is changing.

However, organisms also have the ability to respond to the environments experienced by previous generations through transgenerational phenotypic plasticity (TGP), a process whereby the parental environments alter the expression of phenotypes and genotypes in their progeny. Parental environmental effects can confer adaptive plasticity based on how reliable the signal is, how well the induced phenotypic change aligns with the environment experienced by progeny, and whether the signal persists in both strength and direction across generations (Uller et al. 2013). Nonetheless, transgenerational plasticity can be disfavored if the offspring are a better predictor of their own environment. Under such conditions, theory predicts that the effects of the parental environment will diminish over time, and the organisms will instead be more likely to default to WGP to influence their own phenotypic development (Lachmann and Jablonka 1996). However, when transgenerational effects reliably predict offspring environment, when these responses vary among genotypes, and when there is negligible cost in responding to these cues, TGP can evolve while priming offspring with programming to face new selective conditions despite having not yet experienced it themselves.

Sessile organisms such as plants are particularly vulnerable to the impacts of climate change due to their sedentary lifestyle, and experience strong selective pressures based on their immediate environment. TGP may offer an additional mechanism that contributes to long-term fitness in response to environmental fluctuations (Agrawal et al. 1999). In accessions of

Arabidopsis thaliana, transgenerational effects in response to thermal regimes weakened over time in some genotypes while others were stronger or even directionally opposite (Alvarez et al. 2020), suggesting that transgenerational effects may be genetically dependent, and therefore have the potential to evolve independently.

Transgenerational plasticity (TGP) often involves changes in gene expression. When effects of TGP persist beyond the F2 generation are thought to be potentially mediated by nongenetic (epigenetic) modifications such as DNA methylation, histone modification, or small RNA (sRNA) production (Bell and Hellmann 2019). Because TGP can alter both gene regulation and quantitative trait variation, considering differential gene expression in tandem with QTL mapping is necessary to fully capture the molecular basis of transgenerational effects.

Empirical evidence supports the role of pre-transcriptional regulation in mediating transgenerational responses in the *Mimulus guttatus* species complex. A study on *M. guttatus* revealed that when subjected to simulated herbivory during the parental generation, genes were differently expressed in response to the wounding in the offspring generation (Colicchio et al. 2015a). A later study on *M. guttatus* implicated differential methylation as a mechanistic component of transgenerational plasticity (Colicchio et al. 2015b). Although previous studies have provided some insight into the induction and persistence of transgenerational plasticity, what remains more elusive are the genetic architecture, gene expression, and interaction between the two that constitute it.

Mimulus laciniatus (Phrymaceae)--a species belonging to the *Mimulus guttatus* species complex--is endemic to the Sierra Nevadas, where it spans both a longitudinal gradient and an elevational cline from 1,000 to 3,300 meters (Figure 1). Species that reside in regions that exhibit strong temporal continuity in climatic variables are thought to be good predictors of their offspring environment. The Sierra Nevada Range has been identified as one of the locations in the United States with strong amounts of interannual environmental autocorrelation, and is predicted to yield conditions necessary for the optimal parental effect (Colicchio and Herman 2020). In addition, selective pressures vary locally across this range, resulting in the evolution of divergent phenotypes in *M. laciniatus* (Love and Ferris 2024) and are thus hypothesized to drive divergent expression of transgenerational effects. As a predominantly self-fertilizing species, *M. laciniatus* is expected to retain a higher degree of epigenetic persistence when compared to its

outcrossing counterparts (Wang et al. 2009), which may result in stronger and more reliable signals being transmitted. Therefore, *Mimulus laciniatus* serves as a tractable study system for characterizing the genetic architecture and gene regulation underlying transgenerational plasticity.

This study represents the first effort to characterize the distinct genetic components underlying transgenerational plasticity in *Mimulus laciniatus*. To test the effect of and variance in transgenerationally plastic responses to temperature change, expression must be tested in both similar and contrasting offspring environments (Munir et al. 2001). To do this, we employ a factorial design using both natural populations and Multiparent Advanced Generation Inter-Cross (MAGIC) scheme across 6 parental haplotypes derived from low, mid and high-elevations wherein both are subjected to growth chamber conditions which mimic diurnal patterns experienced by the warmest (H) and coldest (C) regions which the natural populations experience. By performing QTL-mapping and differential gene expression analysis, I seek to answer the following questions: (1) Are there large-effect QTLs that are responsible for conferring organisms with the capacity to shift their position on the fitness landscape? (2) How does the temperature regime experienced by the parental generation shape the offspring transcriptome?

METHODS

Founder Populations

Dr. Jay Sexton collected seed from populations in the Sierra National Forest (SNF) and Yosemite National Park (YNP). Eight parental populations were initially included: Sandy Bluff (SNB), Peterson Road (PET), Shaver Lake (SHL), Dinkey Creek (DNK), Hetch Hetchy Reservoir (HHR), Turtleback Dome (TRT), White Wolf (WLF), and Olmstead Point (OPN). Due to challenges in pollen viability, DNK and WLF populations were excluded after the F4 generation. Each founder population was selected to represent a unique combination of elevation (low, medium, or high) and longitudinal transect (northern or southern) (Figure 2A).

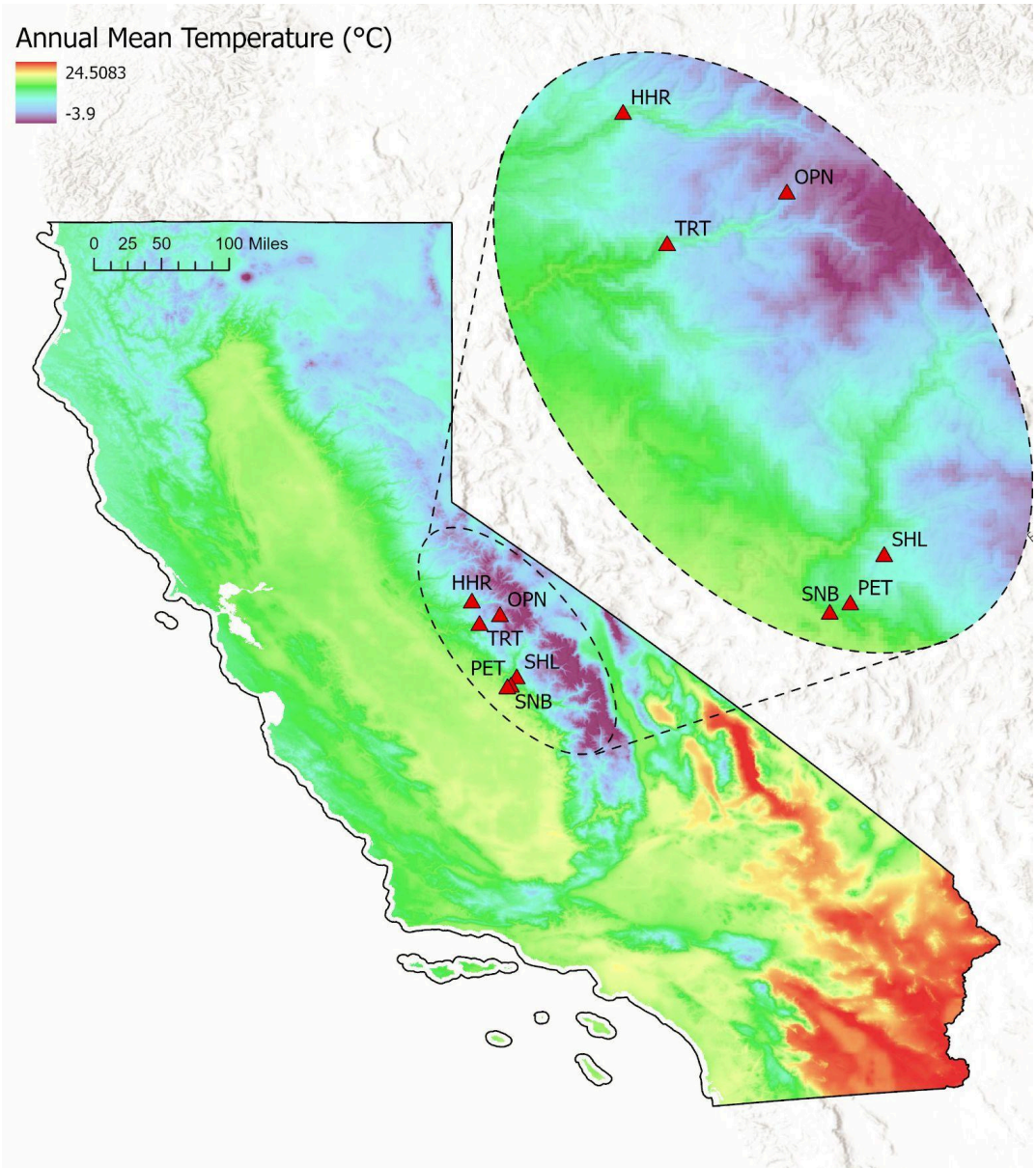

Figure 1. Map of annual mean temperature (BIO1) across California, based on WorldClim v2.1 data (1970-2000; 30 arc-second resolution). Colored raster values represent average annual temperature (°C), with sampling populations of *M. laciniatus* indicated by red triangles.

Table 1. **Geographic coordinates, bioclimatic variables, and elevation for six *Mimulus laciniatus* populations.** Bioclimatic variables were downloaded from WorldClim v2.1 at 30 arc-second resolution, representing 1970-2000 climate averages (https://www.worldclim.org). Variables include: **BIO1** – Annual Mean Temperature (°C), **BIO5** – Maximum Temperature of Warmest Month (°C), **BIO6** – Minimum Temperature of Coldest Month (°C), **BIO12** – Annual Precipitation (mm).

Population	Latitude	Longitude	BIO1	BIO5	BIO 6	BIO12	Elevation (m)
OPN	37.81073	-119.48518	3.78	22.90	-10.60	726.0	2530
SHL	37.1447	-119.306467	10.33	28.20	-1.90	913.0	1595
TRT	37.716	-119.705	10.53	29.30	-2.20	948.0	1481
PET	37.055767	-119.3687	12.92	31.40	0.20	902.0	1257
HHR	37.957183	-119.78595	12.18	30.50	-1.10	907.0	1208
SNB	37.038683	-119.406367	15.00	33.90	1.40	836.0	1004

MAGIC Line Crossing Scheme and Experimental Design

Seed collected from these natural populations was stratified on Fafard 4P potting mix at 4°C in darkness for 10 days. Plants were grown by collaborators in the Duke University greenhouse, watered daily, and fertilized weekly with bloom boost fertilizer. To minimize contamination, plants were grown as far apart from each other as possible.

Using field-collected seeds, Dr. Paivi Leinonen established Multiparent Advanced Generation Inter-Cross (MAGIC) lines (Huang et al. 2011). Initial F1 crosses were performed between the following pairs of inbred founder lines (maternal parent × paternal parent): HHR × OPN, SNB × TRT, and SHL × PET. These F1 plants were then intercrossed in combinations designed to incorporate four parental haplotypes into the resulting F2 lines. The four-way crosses were designated as follows: AL = (HHR × OPN) × (SNB × TRT), CL = (HHR × OPN) × (SHL × PET), and EL = (SHL × PET) × (SNB × TRT); reciprocal crosses were also performed to account for potential maternal effects: AU = (SNB × TRT) × (HHR × OPN), CU = (SHL × PET) × (HHR × OPN), and EU = (SNB × TRT) × (SHL × PET) (Figure 2B).

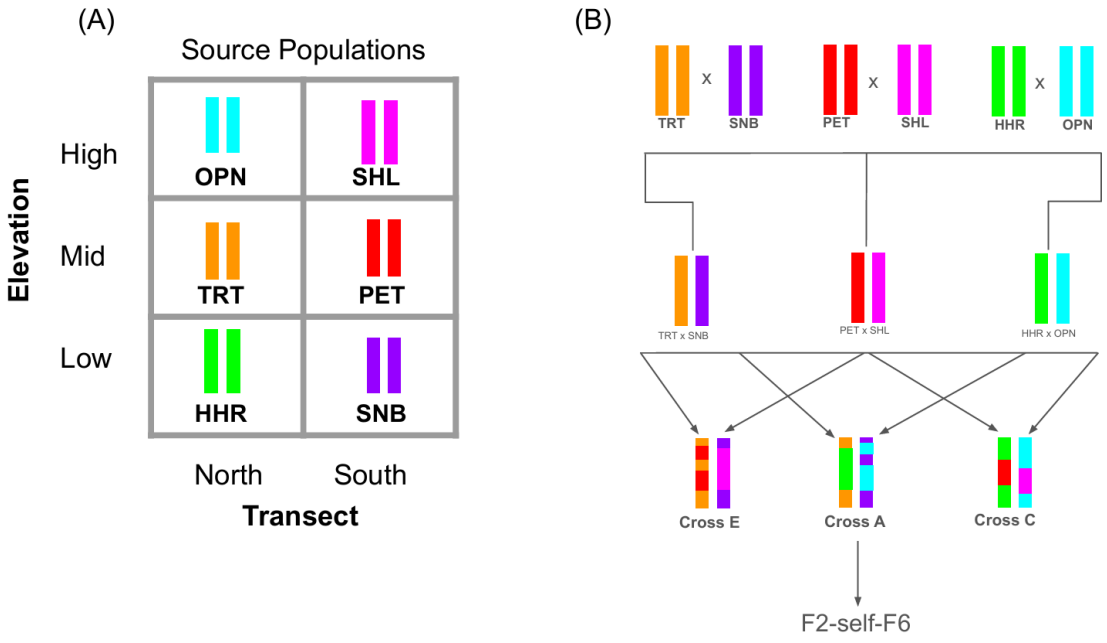

Figure 2. (A) Source populations of *M. laciniatus* arranged by position on the elevational cline and longitudinal transect. (B) Crossing scheme for generating MAGIC lines. F1 crosses were made between paired parental lines, followed by three independent four-way crosses (Crosses E, A, and C). Individuals were selfed from the F2 to F6 generation. For simplicity, reciprocal crosses are not shown here.

Following these crosses, outcrossed F2 plants were then self-pollinated to produce F3 seeds. Because F2 seed counts were low, multiple F3 sublines were initiated per F2 individual, and additional F1s were generated for subsequent crosses (designated as "Set I" and "Set II"). At the F5 generation, plants from Set I and Set II were grown at the same time to synchronize developmental stages and homogenize potential maternal effects on the F6 generation.

During the F7 generation, Dr. Jack Colicchio exposed cross populations to either a hot (H) or cold (C) parental environment, simulating the extreme temperatures experienced by natural populations. Plants were grown under a 16-hour photoperiod in 2’ pots, with hot conditions set at 38°C during the day and 16°C at night, and cold conditions maintained at 24°C for both daytime and nighttime. The resulting F8 generation, derived from self-pollinated F7 individuals, was then grown under either hot (H) or cold (C) offspring environments. This experimental design resulted in a full factorial design, where each cross was grown in: HH = hot parent x hot offspring, CC = cold parent x cold offspring, HC = hot parent x cold offspring, and CH = cold parent x hot offspring.

Phenotypic Trait Measurements

Dr. Jack Colicchio and Cameron Yuki measured a broad set of phenotypic traits thought to be under local selection. Each phenotype was measured for each cross in all four environmental combinations (HC, CC, CH, HH) to capture variation in developmental timing, morphology, pigmentation, and senescence.

Floral Morphology

Flower anthocyanin was scored visually on a scale from 0 (no pigmentation) to 5 (strong pigmentation) on the ventral petal of the first flower. Corolla width was measured as the width of the first flower, in 1/100th of an inch, between lateral petals. Tube length was measured as the distance from the peduncle to the junction of the dorsal and lateral petals, in 1/100th of an inch. Peduncle length was measured from the stem to the calyx base in 1/100th of an inch.

Vegetative Traits

Petiole length was measured as the distance from the stem to the blade, in 1/100th of an inch. Leaf length was measured as total length from the petiole base to the tip of the leaf blade, in 1/100th of an inch. Whole-petiole was measured as the length of the leaf blade only, excluding the petiole. Leaf width was measured as the maximum blade width (uninterrupted by lobing), in 1/100th of an inch.

Architectural Traits

The height of flowering was measured as the vertical height from the soil surface to the shoot apical meristem, on the first day the first flower bloomed.

Trichome Traits

Top G trichomes were measured as glandular trichome count across a transverse fold on the upper leaf surface. Bottom G trichomes were measured as glandular trichome count across a

transverse fold on the lower leaf surface. Top NG trichomes were measured as non-glandular trichome count across a transverse fold on the upper leaf surface. Bottom NG trichomes were measured as non-glandular trichome count across a transverse fold on the lower leaf surface.

Phenology

The node to flower was measured as the node number at which the first flower emerged (0 = cotyledon, 1 = first true leaves, etc.). The first day to flower was recorded as the date when the first flower opened.

For each quantitative trait, plasticity was calculated as follows:

$$WGP(Cold) = Trait\,Value(CH) - Trait\,Value(CC)$$

$$WGP(Hot) = Trait\,Value\,(HC) - Trait\,Value\,(HH)$$

$$WGP = (WGP(Cold) + WGP(Hot))/2$$

$$TGP(Cold) = Trait\,Value(HC) - Trait\,Value\,(CC)$$

$$TGP(Hot) = Trait\,Value(HH) - Trait\,Value\,(CH)$$

$$TGP = (TGP(Cold) + TGP(Hot))/2$$

DNA Extraction and Sequencing

Dr. Jack Colicchio and Cameron Yuki collected leaf tissue from both inbred parental lines and recombinant inbred line panels (MAGIC lines), totaling nine plates with approximately four replicates per line. MAGIC DNA was extracted using a modified CTAB protocol (Kelly and Willis 1998) with salt wash and RNaseA treatment, while founder DNA was extracted using the GeneJet kit (ThermoFisher). Whole-genome sequencing of inbred founder lines was conducted at approximately 8× depth using Illumina sequencing. In addition, 800 MAGIC line individuals were sequenced using double-digest Restriction-site Associated DNA sequencing (ddRAD-seq), at approximately 2x depth.

Linkage Construction and QTL Mapping

I indexed the *M. laciniatus* assembly (daEryLaci1.0.pri, GenBank accession GCA_040207155.1) using GATK (version 4.2.6.1; McKenna et al., 2010). I then created the accompanying sequence dictionary and index files using CreateSequenceDictionary and samtools faidx. Next, I trimmed adapter sequences ligated during library preparation from all samples using Trimmomatic. After adapter trimming, I aligned and cleaned reads to the reference genome using the BWA-MEM algorithm (Li, 2013). For founders represented in the MAGIC line crossing scheme, I marked PCR duplicates using GATK's MarkDuplicates. However, I did not perform this duplicate-marking step for ddRAD-seq data, because PCR duplicates cannot be reliably distinguished from genuine variant sites in this sequencing method.

I then performed variant calling using GATK's HaplotypeCaller in GVCF mode, specifying a heterozygosity prior of 0.00555. This heterozygosity estimate was derived from GenomeScope's analysis of the k-mer spectrum of raw sequencing reads from the same individual used to generate the reference assembly (Figure 3). For validation, I ran HaplotypeCaller on founder HHR with both 0.00555 and 0.02 priors (the latter commonly used for outcrossing species *M. guttatus*), but found that through IGViewer visualization, the Bayesian prior did not significantly affect the quality or quantity of discovered variants.

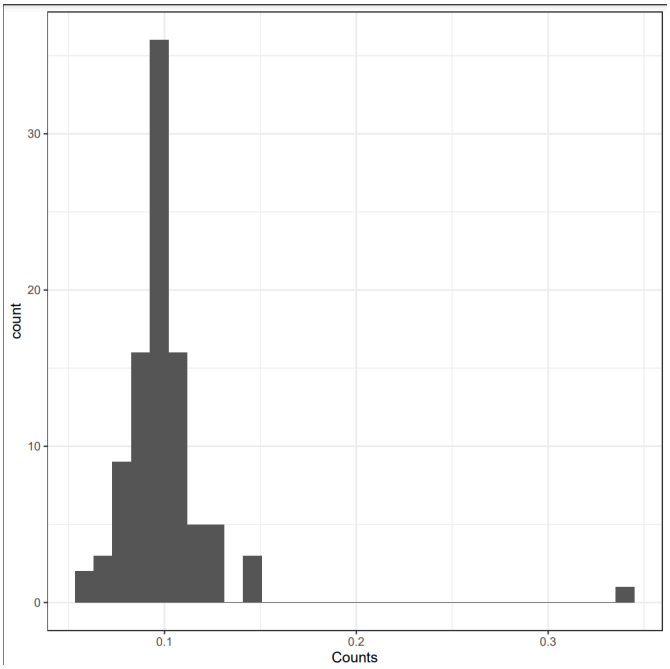

Figure 3. Histogram of k-mer frequencies generated by GenomeScope from the assembly genome. The k-mer spectrum reflects the distribution of unique and repetitive sequences and was used to estimate a heterozygosity prior for variant discovery.

Following variant calling, I imported the resulting GVCFs from the six inbred founder individuals and approximately 800 MAGIC line samples into separate GenomicsDB workspaces. I then performed joint genotyping on each workspace using GATK's GenotypeGVCFs, producing two group-specific VCFs. From this, I extracted only single-nucleotide polymorphism (SNPs) from each VCF using GATK's SelectVariants, explicitly omitting any insertion-deletion (indel) variants. I subsequently applied two rounds of variant filtering, following GATK's recommended standard filters, and enforced a minor allele frequency (MAF) threshold of ≥ 0.05. After filtering, I removed any contigs with <2 markers because inter-marker distances could not be calculated on a single marker. An overview of the complete variant calling and filtering workflow is provided in Figure 4.

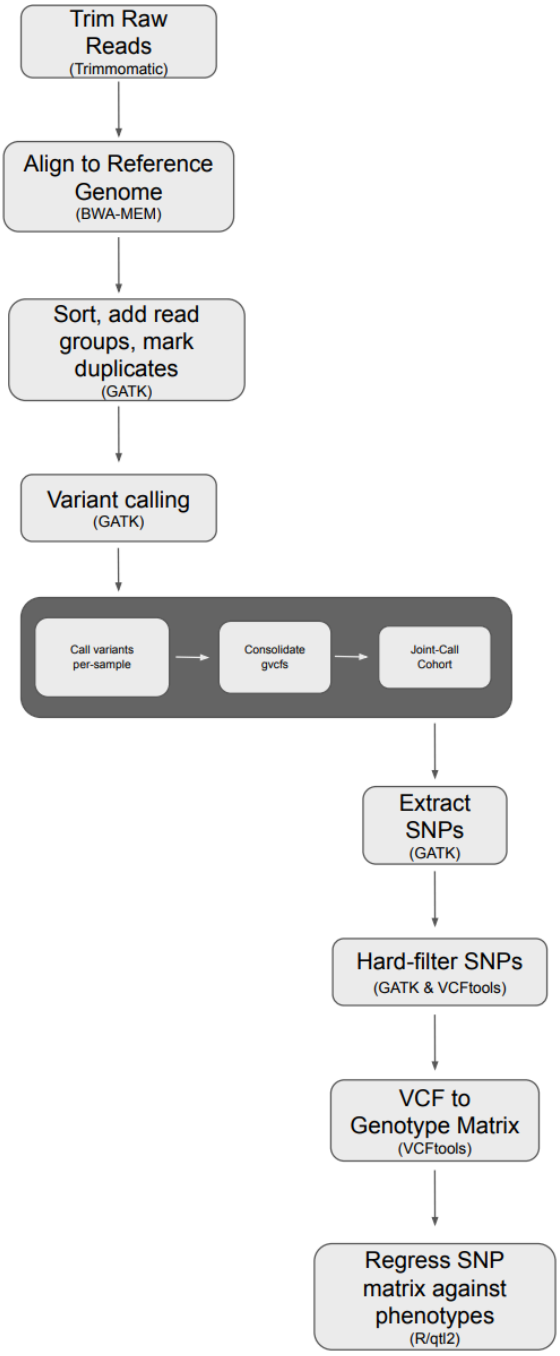

Figure 4. Overview of the variant calling and genotyping workflow. Raw reads were processed, aligned to the reference genome, and prepared for GATK variant calling. From these resulting files, SNPs were extracted, filtered, and encoded as a genotype matrix.

Using VCFtools' Genotype012 format (Danecek et al., 2011), I encoded filtered variant calls into genotype matrices with allele codes as follows: A (homozygous reference), H (heterozygous), and B (homozygous alternate). I performed an initial inner join to identify

informative SNPs shared between the inbred founder panels and MAGIC line genotype matrices (crosses A, E, C). After subsetting genotype data by cross, I removed invariant sites within each population and performed a second inner join between all crosses to retain only SNPs polymorphic in all crosses.

Phenotypic and genotypic data were analyzed using R/qtl2 for QTL mapping. Because R/qtl2 does not natively support six-founders for linkage map estimation, I subset the genotypic data by cross groups to treat each as a four-way mapping population. For each cross, I re-estimated inter-marker distances based on recombination frequencies using R/qtl2's est_map() function. These individual linkage maps were then combined into a consensus map using R/LPmerge, weighting each map proportionally according to sample representation. I then performed single-QTL genome scans for each quantitative phenotype and associated plasticity values using R/qtl2's scan1() function to calculate logarithmic of the odds (LOD) scores, and I determined genome-wide significance thresholds by performing 1,000 permutations. This approach facilitated the identification of quantitative trait loci (QTLs) by leveraging the genetic structure and recombination events inherent in the MAGIC lines.

Natural Populations and Experimental Design

The natural populations represented in this second aim corresponded to the same founding individuals included in the MAGIC line crossing scheme (Table 1). Dr. Jack Colicchio randomly selected seeds from each of the six natural populations and grew them in a growth chamber under a 16-hour photoperiod. Plants were cultivated in 2″ pots at 38°C during the day and 16°C at night to simulate hot conditions, and at 24°C for both daytime and nighttime to simulate cold conditions. Each of the F0 populations was grown under either hot or cold environmental conditions, after which self-fertilized seeds were collected. The resulting F1 seeds were then grown under cold offspring environments. This experimental design resulted in two environmental combinations for each population: cold parent, cold offspring (CC), and hot parent, cold offspring (HC), allowing us to test the effect of one extreme parental environment on offspring gene expression.

RNA Extraction and Sequencing

Dr. Jack Colicchio and I extracted RNA from 42 samples of leaf tissue using the Zymo Direct-Zol TRIzol method. These samples represented at least three biological replicates per growth condition (HC, CC) within each of the six populations (SNB, TRT, HHR, SHL, OPN, PET), resulting in a total of 12 experimental classes. I sent RNA samples to Novogene, where libraries were prepared using the AB Clonal kit and sequenced on an Illumina NovaSeq XPlus platform at a depth of approximately 20 million reads per sample.

Mapping, Read Count, and Modeling

I removed adapters ligated during library preparation using Fastp software (Chen et al., 2018) to ensure high-quality reads for downstream analysis. Due to the lack of a comprehensive annotation for the *Mimulus laciniatus* genome, I indexed and aligned cleaned reads against the annotated *Mimulus nasutus* var. SF v2.1 using the splice-aware STAR aligner (Dobin et al., 2012). I extracted gene-level expression counts from the second column (unstranded read counts) of STAR's automatically generated ReadsPerGene.out.tab file and compiled these counts into a matrix across all samples. I filtered this count matrix to retain genes with a total of at least 10 reads across all samples, reducing the gene set from 25,116 to 22,090 genes. An overview of the complete differential gene expression workflow is provided in Figure 5.

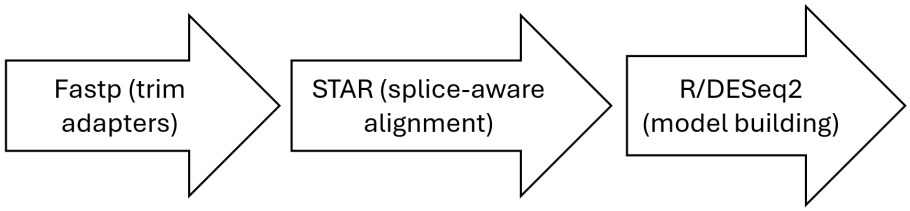

Figure 5. Overview of differential gene expression workflow. Reads were processed with Fastp, aligned to the reference genome, and gene counts were extracted for modeling.

Using R/DESeq2, I constructed two models for differential expression analysis: (1) design = ~ + population + batch + condition (Figure 6A & B) to evaluate the global effect of the experimental condition gene expression, and (2) design = ~ + population + batch + condition + condition: population (Figure 6C) to test whether the effect of condition on gene expression varied by population.

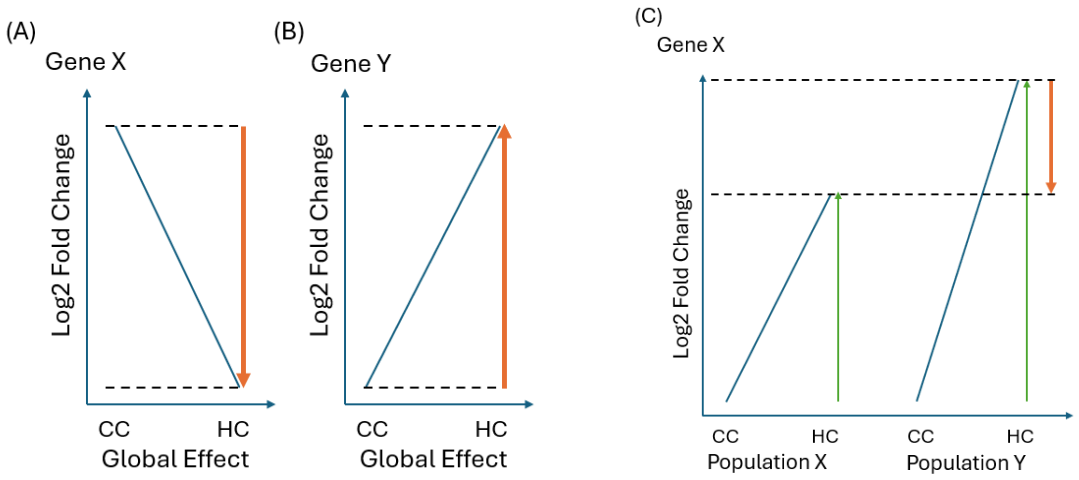

Figure 6. Simplified representations of two differential gene expression models. (A & B) Model 1 depicts global effects of heat, with downregulation of Gene X (A) and upregulation of Gene Y (B) observed across populations. (C) Model 2 illustrates a genotype × environment interaction, where Gene X is more strongly downregulated by heat in Population Y than in Population X. The direction of differential gene expression is indicated by the orange arrow.

Because extractions were performed on different dates, I encoded each extraction group alphabetically as a batch variable in the design matrices to control for potential batch effects. For each model, I conducted a likelihood ratio test (LRT) to evaluate the significance of each variable, retaining only those that significantly improved the fit of the model. For functional inference, I retrieved peptide sequences for significantly differentially expressed genes (adjusted p-value < 0.05) from Phytozome and used BLASTP to compare them to the *Arabidopsis thaliana* Araport11 protein database via TAIR, assigning each peptide to the homolog with the lowest E-value to infer putative functional annotations.

RESULTS

Inflated Genetic Map

Across all contigs, the length of the genetic map is higher than anticipated by thousands of cM. In all contigs except 63 and 76--which have the fewest number of markers--cross E seems to have higher inflation when compared to crosses A and C (Figure 7). Due to this unanticipated distortion, we rescaled the physical map assuming a constant rate of recombination and a total length of 2000 cM.

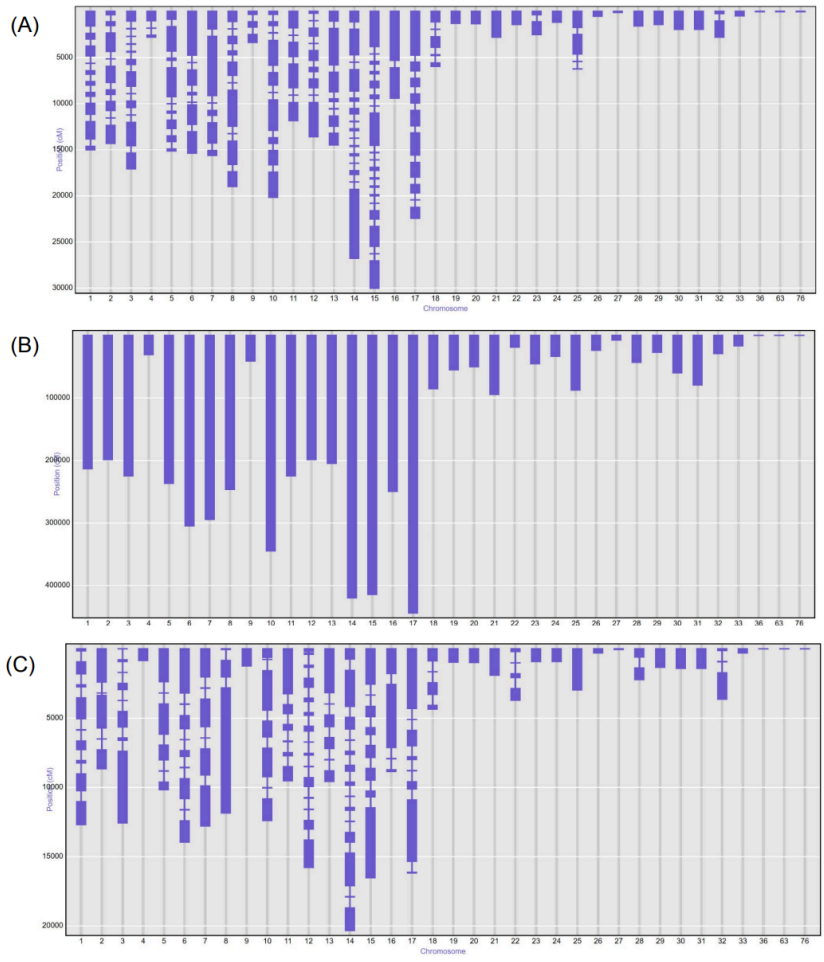

Figure 7. Genetic map displaying marker density along contigs. The x-axis represents contigs, and the y-axis shows genetic positions in centiMorgans (cM). (A) Corresponds to Cross A, (B) corresponds to Cross E, and (C) corresponds to Cross C.

Genetic Architecture of Floral Traits and Temperature-Dependent Plasticity

Our results did not indicate any significant QTL for transgenerational plasticity. However, we did identify significant QTL for phenotypic variation in mean flower anthocyanin, corolla width, and tube length (Figures 8-10). We also detected significant QTL for within-generation plasticity (WGP) in flower anthocyanin under cold conditions and in corolla width under hot conditions (Figures 11, 12). Notably, all QTL for phenotypic trait variation were detected exclusively under conditions in which both the parental and offspring generation experienced cold (CC). Except for WGP(Hot) corolla width, all traits included at least one QTL region on contig 12. Although most QTL intervals showed minimal overlap, mean flower anthocyanin (CC) [0.042142-3.131661] and WGP(Cold) flower anthocyanin [0.042142-3.312962] share a nearly identical QTL region (Table 2). Because WGP was only detected for two traits under different temperature regimes, our results suggest that within-generation plasticity is temperature-dependent: plasticity in flower anthocyanin is associated with a genomic region response to cold offspring environments (CH vs. CC), whereas plasticity in corolla width is linked to a region responsive to hot offspring environments (HC vs. HH).

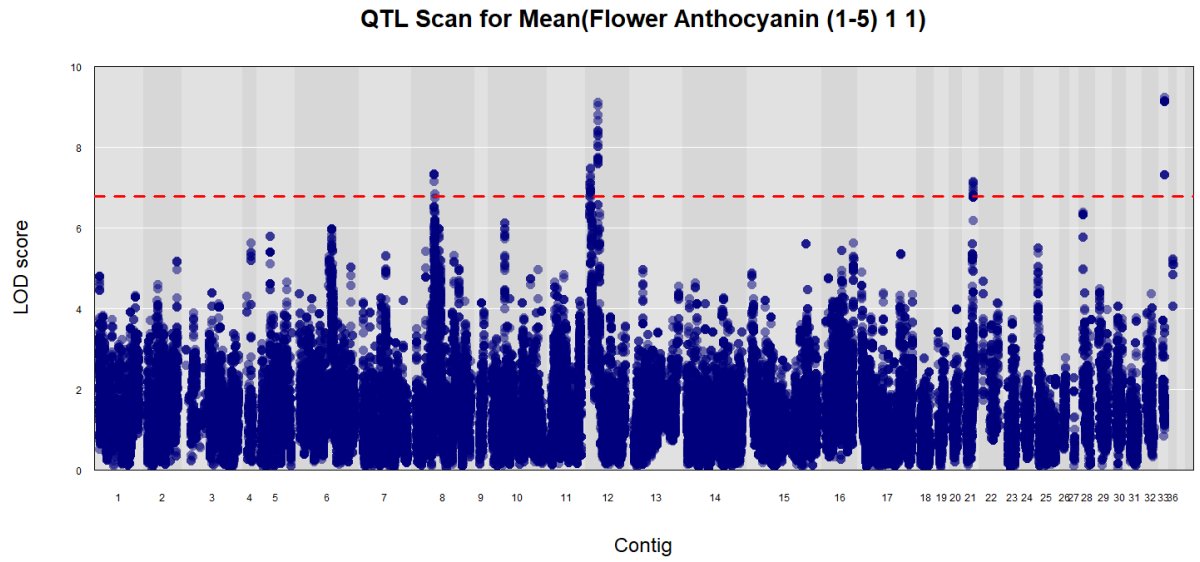

Figure 8. QTL map plotting of genome-wide LOD scores for flower anthocyanin (CC). The dashed red line represents the statistical significance threshold determined via a permutation test at α = 0.05. The statistical significance threshold determined via a permutation test for mean flower anthocyanin (CC) at α = 0.05 was 6.77.

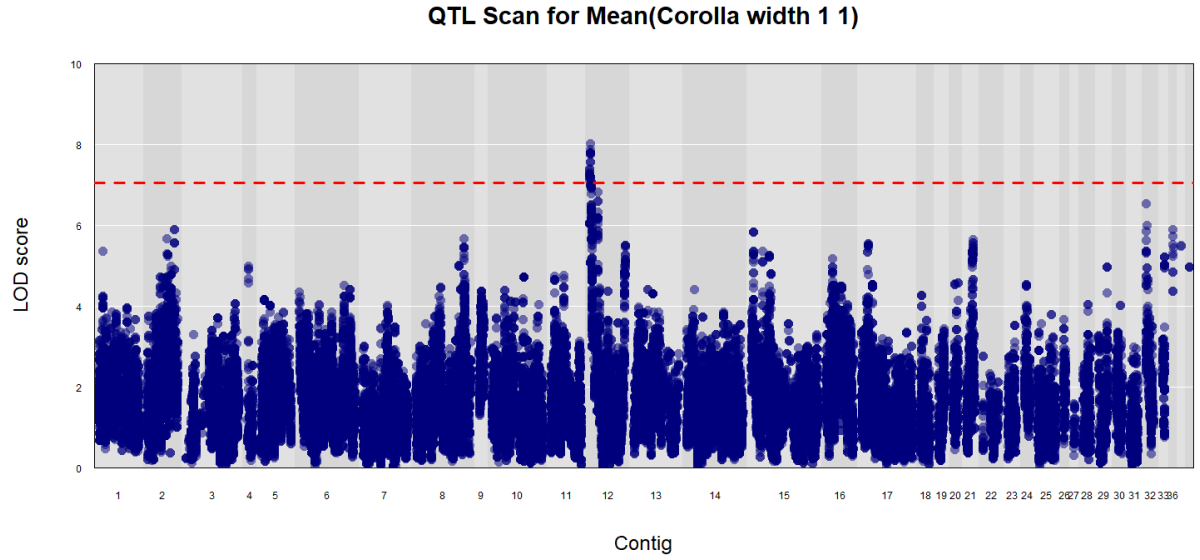

Figure 9. QTL map plotting of genome-wide LOD scores for mean corolla width (CC). The dashed red line represents the statistical significance threshold determined via a permutation test at α = 0.05. The statistical significance threshold determined via a permutation test for mean corolla width (CC) at α = 0.05 was 7.04.

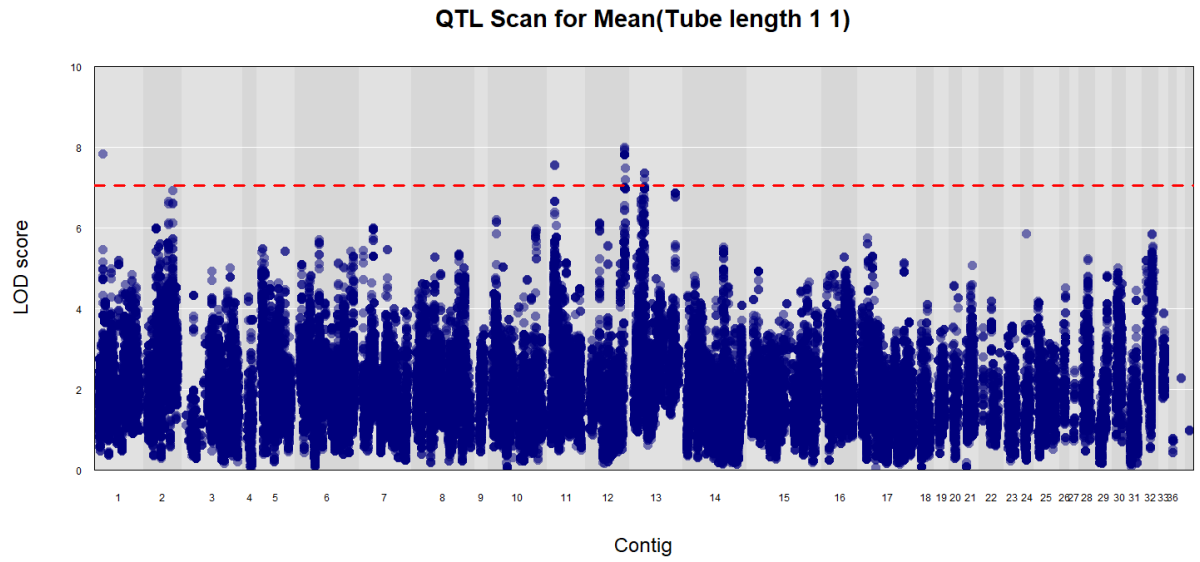

Figure 10. QTL map plotting of genome-wide LOD scores for mean tube length (CC). The dashed red line represents the statistical significance threshold determined via a permutation test at α = 0.05. The statistical significance threshold determined via a permutation test for mean tube length (CC) at α = 0.05 was 7.05.

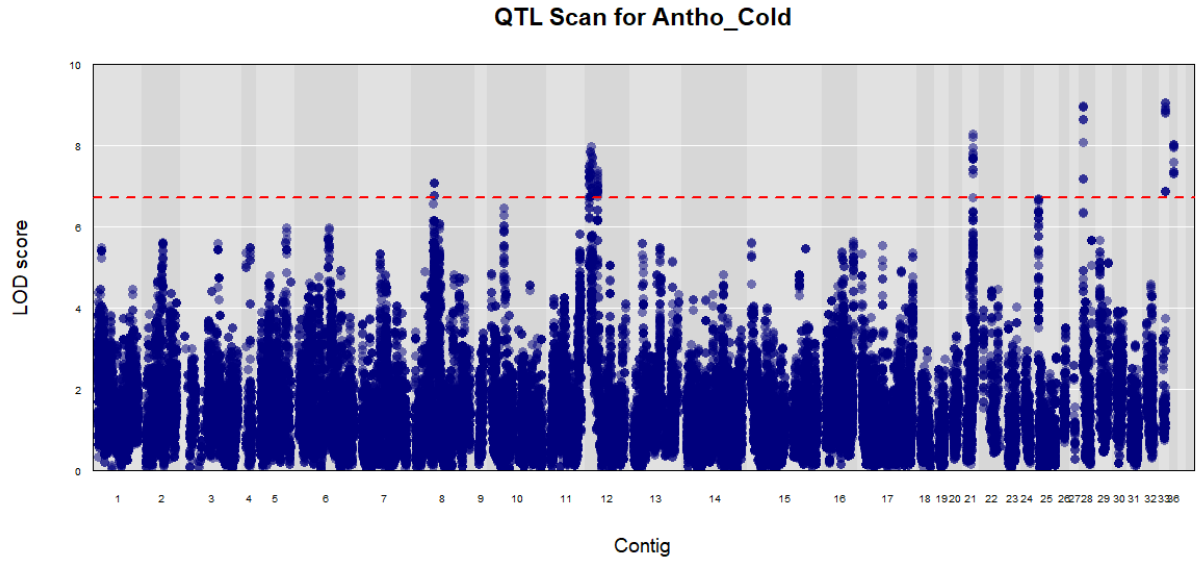

Figure 11. QTL map plotting of genome-wide LOD scores for WGP(Cold) floral anthocyanin. The dashed red line represents the statistical significance threshold determined via a permutation test at α = 0.05. The statistical significance threshold determined via a permutation test for WGP(Cold) floral anthocyanin at α = 0.05 was 6.72.

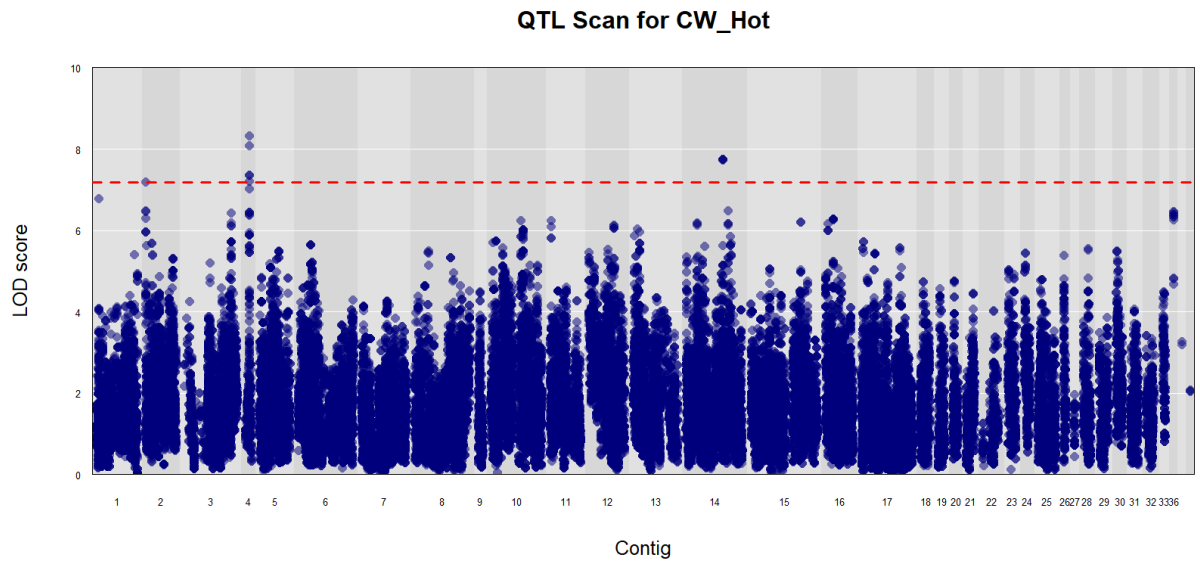

Figure 12. QTL map plotting of genome-wide LOD scores for WGP(Hot) mean corolla width. The dashed red line represents the statistical significance threshold determined via a permutation test at $\alpha = 0.05$. The statistical significance threshold determined via a permutation test for WGP(Hot) corolla width at $\alpha = 0.05$ was 7.18

Table 2. Summary of all traits with significant QTL detected. For each trait, the associated contig, peak QTL position in centiMorgans (cM), LOD score at the peak, and the lower (CI_low) and upper (CI_high) bounds of the 1.5-LOD support interval are described. An asterisk (*) indicates the peak with the highest confidence for the given trait, from which founder allele effects were estimated.

Trait	Contig	Position (cM)	LOD	CI_low	CI_high
Mean Flower Anthocyanin (Cold x Cold)	8	6.786246	7.337892	6.731770	8.75562
Mean Flower Anthocyanin (Cold x Cold)	12*	3.126242	9.114631	3.016522	3.312962
Mean Flower Anthocyanin (Cold x Cold)	21	2.340182	7.51321	2.279605	2.377374
Mean Corolla Width (Cold x Cold)	12*	0.129265	8.01559	0.042142	3.131661
Mean Tube Length (Cold x Cold)	11	1.278115	7.563278	1.247769	1.301077
Mean Tube Length (Cold x Cold)	12*	12.818674	7.995351	12.818295	12.991616
Mean Tube Length (Cold x Cold)	13	3.863834	7.362574	2.810794	15.233812
WGP(Cold) Flower Anthocyanin	8	7.174686	7.072771	6.731770	9.160313

Table 2. Continued.

Trait	Contig	Position (cM)	LOD	CI_low	CI_high
WGP(Cold) Flower Anthocyanin	12	0.900110	7.985894	0.042142	3.312962
WGP(Cold) Flower Anthocyanin	21	2.340182	8.274685	2.279605	2.359429
WGP(Cold) Flower Anthocyanin	28*	0.001103	8.987240	0.001103	0.022058
WGP(Cold) Flower Anthocyanin	33	0.822726	9.042199	0.818905	0.822731
WGP(Hot) Corolla Width	4*	1.725569	8.324681	1.703469	1.741897

Within the most significant QTL for each trait, we observed variation in the allelic effect sizes of individual founders on both trait expression and within-generation plasticity (WGP). Under an additive model, the SNB founder consistently contributed positively to plasticity, increasing mean trait values for both flower anthocyanin in WGP(Cold) and corolla width in WGP(Hot) (Figure 13D-E). In contrast, founders OPN, PET, and SHL consistently showed negative contributions to both forms of plasticity (Figure 13D-E). Interestingly, the direction of founder effects for HHR and TRT reversed direction for within-generation plasticity depending on the trait and the environmental context: HHR had a positive effect on flower anthocyanin plasticity in WGP(Cold) but a negative effect on corolla width plasticity in WGP(Hot), while TRT showed the opposite pattern (Figure 13D-E).

Among traits measured under the cold parental x cold offspring environment, mean corolla width exhibited less allelic variation: OPN, PET, and SHL had near-zero influence on trait variation, SNB had a slightly negative effect, and HHR and TRT had slightly positive contributions (Figure 13B). In contrast, mean flower anthocyanin (CC) showed greater allelic variation: only OPN and SNB contributed negatively, while other founders had neutral or positive effects on mean trait values (Figure 13A). For mean tube length (CC), founder effect sizes for OPN, PET, and SHL mirrored the negative contributions observed in their plasticity patterns, consistently reducing mean trait values across conditions (Figure 13C).

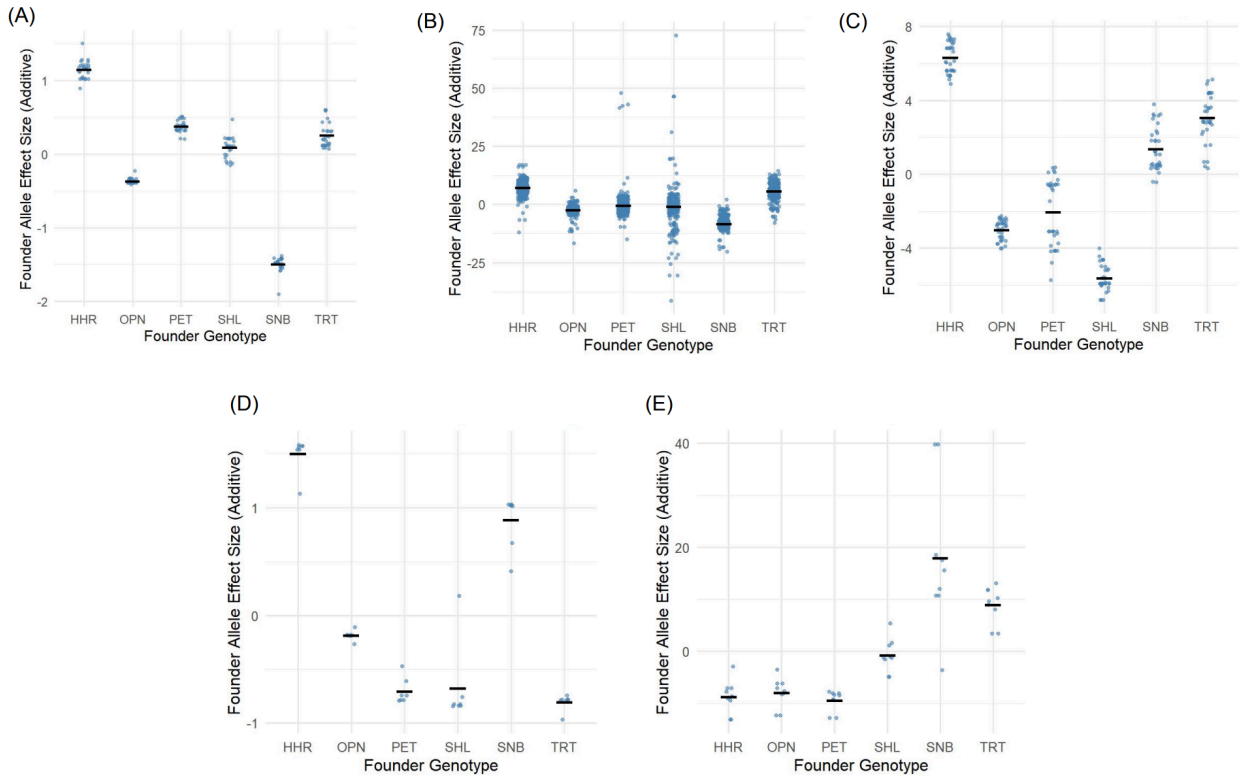

Figure 13. Estimated founder allele effect sizes. (A) mean flower anthocyanin (Cold x Cold) at QTL peak on contig 12, (B) mean corolla width (Cold x Cold) at QTL peak on contig 12, (C) mean tube length (Cold x Cold) at QTL peak on contig 12, (D) flower anthocyanin WGP(Cold) at QTL peak on contig 28, and (E) mean corolla width WGP(Hot) at QTL peak on contig 4. Effect sizes were calculated using an additive model for all markers within the 1.5 LOD support interval, corresponding to an approximate 95% confidence interval around the peak.

RNA-Seq Reveals Population Clustering

Principal component analysis (PCA) revealed partial patterns of population structure in gene expression (Figure 14). To reduce the high-dimensionality of our gene expression dataset and identify population- and treatment-specific variation, I performed PCA on variance-stabilized and batch-effect-corrected data. PC1 and PC2 explained 27% and 23% of the total variance, respectively. Along PC1, population HHR, which originates from the lowest elevation in the northern transect, clustered distinctly away from other populations. Along PC2, population SNB, which also originates from the lowest elevation but in the southern transect, is also clustered separately. In contrast, PET and SHL, both southern transect populations, clustered closely

together in PCA space. Within each population, HC and CC treatment groups did not form distinct clusters, indicating limited separation by treatment within populations in PCA space.

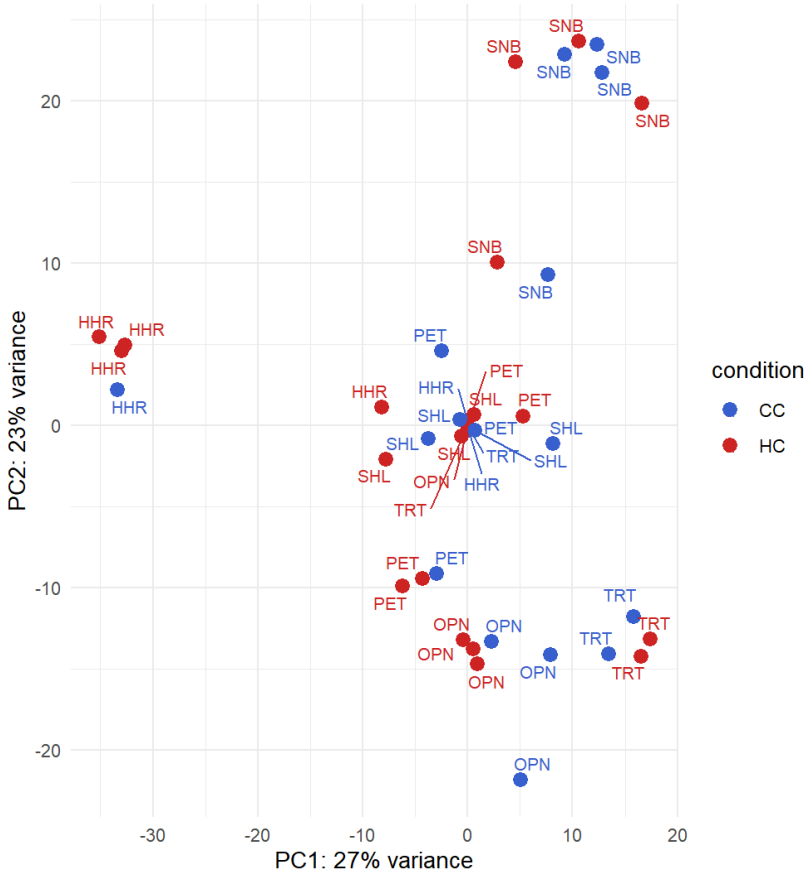

Figure 14. Principal component analysis (PCA) of gene expression data from natural populations. Each point represents an individual sample, projected along the first two principal component axes (PC1, PC2). Red points indicate individuals whose parents were exposed to heat (HC), while blue points represent those from control (CC) parental environments.

Parental Heat Exposure Alters Offspring Gene Expression

Differentially expressed genes (DEGs) were identified between treatment conditions and across populations, with differences observed in the magnitude and direction of expression changes. In the assessment of global patterns of differential gene expression between treatment conditions, we examined an MA plot generated from the model ~ *population* + *batch* + *condition*. This model tested the effect of experimental conditions (HC vs. CC) on gene expression, while controlling for population and batch effects. The MA plot revealed significant differential expression between conditions (Figure 15A).

Although some genes were upregulated, most DEGs exhibited downregulation in the HC condition as indicated by a negative log2 fold change. To evaluate variation in gene expression responses across populations, a second MA plot was generated from model ~ *population* + *batch* + *condition* + *condition:population*, which was used to evaluate how gene expression responses to the HC condition varied across populations. In this model, comparisons between populations reveal differentially expressed genes more frequently upregulated in one population compared to another (Figure 15B).

In both models, genes with lower average expression levels (log counts < 1e+01) exhibited greater variance in $\log_2$ fold change, and fewer of these low-expression genes were identified as significantly differentially expressed.

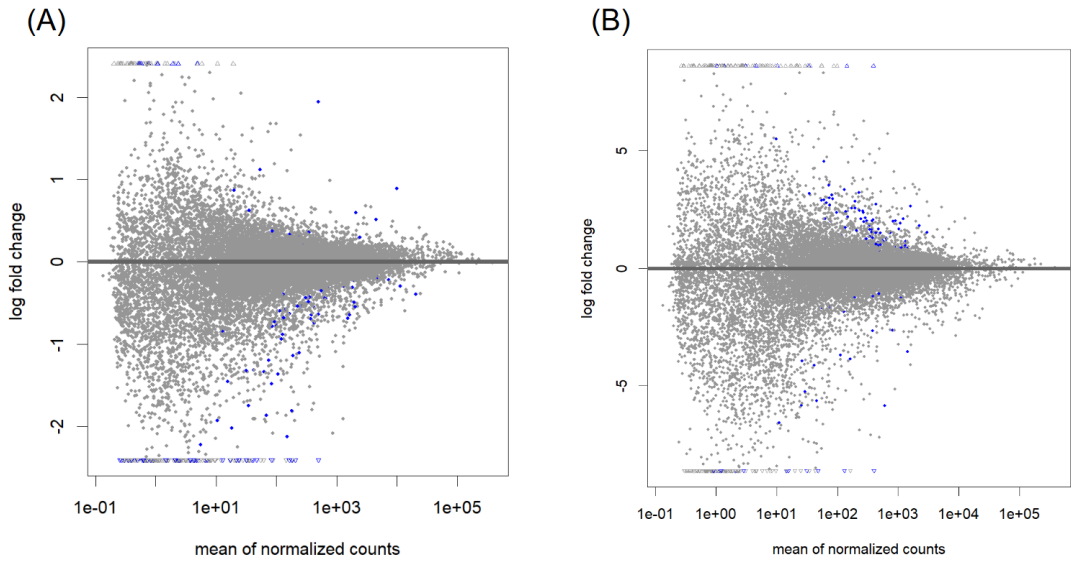

Figure 15. MA-plots displaying differential gene expression results. Each point represents a gene; those highlighted in blue are significantly differentially expressed (adjusted p-value < 0.05). (A) Comparison of heat-treated versus control samples, and (B) pairwise comparisons between populations under heat-treated conditions.

Table 3. Genes upregulated in offspring following parental heat exposure. Transcript IDs represent the first isoform of each differentially expressed gene from the *Mimulus nasutus* annotation. The Arabidopsis homolog indicates the most similar (e-value) gene in *Arabidopsis thaliana*. Log_2 fold change reflects the magnitude of expression change in offspring, and adjusted p-values account for multiple testing ($\alpha = 0.05$).

Transcript ID	Araport11 Homolog	Physical Location	Log2 FC	P-value adj.
Minas.08G242600	bZIP44 (basic leucine-zipper 44)	Chr_08:24138206..24138713 reverse	12.36453	2.43E-06
Minas.05G045000	Peroxidase superfamily protein	Chr_05:2279899..2281467 reverse	18.57331	0.000484
Minas.14G080300	SPT16 (global transcription factor C)	Chr_14:5794539..5798754 reverse	15.12106	0.002807
Minas.10G171500	CYP93D1 (cytochrome P450, family 93, subfamily D, polypeptide 1)	Chr_10:21210071..21212136 forward	16.18714	0.006985

Table 3. Continued.

Transcript ID	Araport11 Homolog	Physical Location	Log2 FC	P-value adj.
Minas.14G188700	A9	Chr_14:18658978..18659555 forward	0.891581	0.007131
Minas.05G000700	PMEAMT (phosphoethanolamine N-methyltransferase)	Chr_05:44675..45822 reverse	15.9914	0.007575
Minas.13G042200	WAK1 (cell wall-associated kinase 1)	Chr_13:6390061..6398673 reverse	16.00326	0.007575
Minas.11G022000	JMJ31 (JUMONJI DOMAIN-CONTAINING PROTEIN 31)	Chr_11:930569..935915 forward	0.235715	0.016193
Minas.09G122000	ARID5 (AT-RICH INTERACTING DOMAIN5)	Chr_09:26528854..26534473 reverse	0.183465	0.023782
Minas.03G126400	AGL12 (AGAMOUS-LIKE 12)	Chr_03:21098956..21101186 forward	14.61284	0.024442
Minas.11G015200	NPF3.1 (NRT1/ PTR FAMILY 3.1)	Chr_11:620506..624319 forward	0.600177	0.025002
Minas.11G059600	NPY8	Chr_11:2932586..2936592 reverse	0.296621	0.029059
Minas.10G103600	MTERF15 (MITOCHONDRIAL TRANSCRIPTION TERMINATION FACTOR 15)	Chr_10:7603520..7605778 forward	1.118737	0.039237

Table 4. Genes downregulated in offspring following parental heat exposure. Transcript IDs represent the first isoform of each differentially expressed gene from the *Mimulus nasutus* annotation. The Arabidopsis homolog indicates the most similar (e-value) gene in *Arabidopsis thaliana*. Log_2 fold change reflects the magnitude of expression change in offspring, and adjusted p-values account for multiple testing ($\alpha = 0.05$).

Transcript ID	Araport11 Homolog	Physical Location	Log2 FC	P-value adj.
Minas.12G098000	VIK (VH1-INTERACTING KINASE)	Chr_12:16917402..16922039 forward	-13.051	1.55E-13
Minas.11G052800	TIM17-2 (translocase inner membrane subunit 17-2)	Chr_11:2542848..2543472 forward	-29.3637	1.59E-11
Minas.04G125500	RPP13 (RECOGNITION OF PERONOSPORA PARASITICA 13)	Chr_04:7040133..7046764 reverse	-8.6207	2.25E-11
Minas.04G208300	CBF1 (C-REPEAT/DRE BINDING FACTOR 1)	Chr_04:20949098..20950067 forward	-21.0346	3.89E-05
Minas.10G132500	GAE1 (UDP-D-GLUCURONATE 4-EPIMERASE 1)	Chr_10:18577279..18579126 reverse	-0.6881	3.89E-05
Minas.14G044700	PDF1.4	Chr_14:2336741..2337071 forward	-20.2906	9.48E-05
Minas.01G082800	CDR1 (CONSTITUTIVE DISEASE RESISTANCE 1)	Chr_01:4760505..4762200 reverse	-20.0943	0.000106
Minas.14G291200	JP630	Chr_14:25567204..25568460 forward	-9.73888	0.000214
Minas.06G112300	CBF2 (C-REPEAT/DRE BINDING FACTOR 2)	Chr_06:5275107..5275991 forward	-15.0291	0.000243
Minas.02G003100	LHT4 (LYSINE HISTIDINE TRANSPORTER 4)	Chr_02:153397..156127 forward	-18.8219	0.000372
Minas.10G008500	PRA1.B4 (PRENYLATED RAB ACCEPTOR 1.B4)	Chr_10:327593..328256 reverse	-0.45079	0.001455

Table 4. Continued.

Transcript ID	Araport11 Homolog	Physical Location	Log2 FC	P-value adj.
Minas.02G141200	DAD1 (DEFECTIVE ANTHER DEHISCENCE 1)	Chr_02:18875835..18877182 forward	-17.5935	0.00159
Minas.04G069900	NHL13 (NDR/HIN1-LIKE 13)	Chr_04:3227665..3228798 reverse	-1.48548	0.001874
Minas.08G203200	XTH15 (xyloglucan endotransglucosylase/hydrolase 15)	Chr_08:20283088..20284455 forward	-1.86846	0.002257
Minas.13G147700	ATHCYSTM4 (CYSTEINE-RICH TRANSMEMBRANE MODULE 4)	Chr_13:21812058..21812739 forward	-3.15987	0.003018
Minas.06G075300	RDUF1 (RING AND DOMAIN OF UNKNOWN FUNCTION 1117 1)	Chr_06:3372076..3374058 forward	-0.32805	0.006038
Minas.03G011000	PAB3 (POLY(A) BINDING PROTEIN 3)	Chr_03:1617807..1622202 reverse	-16.2174	0.006985
Minas.14G270300	PAE11 (PECTIN ACETYLESTERASE 11)	Chr_14:24653359..24656066 reverse	-11.6139	0.006985
Minas.05G030900	RAV1 (RELATED TO ABI3/VP1 1)	Chr_05:1502142..1503612 forward	-1.81354	0.007126
Minas.07G058800	KAB1 (potassium channel beta subunit 1)	Chr_07:3544290..3547612 forward	-0.23323	0.007131
Minas.13G012000	WDR26	Chr_13:711279..713474 reverse	-15.8985	0.008403
Minas.06G083600	RPF1 (RNA processing factor 1)	Chr_06:3876956..3879562 forward	-15.8743	0.008403
Minas.10G152500	VQ24	Chr_10:20140644..20141869 forward	-1.36598	0.008403

Table 4. Continued.

Transcript ID	Araport11 Homolog	Physical Location	Log2 FC	P-value adj.
Minas.01G062000	WRKY41	Chr_01:3343903..3345286 forward	-1.31743	0.009784
Minas.08G097900	ACT7 (ACTIN 7)	Chr_08:7634436..7637295 forward	-0.21664	0.009784
Minas.07G110700	MFDX1 (MITOCHONDRIAL FERREDOXIN 1)	Chr_07:23067138..23068388 forward	-15.6521	0.010093
Minas.14G062000	MCU2 (MITOCHONDRIAL CALCIUM UPTAKE2)	Chr_14:3544771..3547005 forward	-0.48701	0.011997
Minas.05G088200	CYP706A3 (cytochrome P450, family 706, subfamily A, polypeptide 3)	Chr_05:20274604..20276956 forward	-3.59411	0.013622
Minas.04G142300	LRR4 (LEUCINE RICH REPEAT PROTEIN 1)	Chr_04:14522713..14525852 reverse	-4.66768	0.014611
Minas.02G050500	GTE7 (global transcription factor group E7)	Chr_02:2342227..2345262 forward	-0.22126	0.016248
Minas.07G108800	NPF7.2 (NRT1/ PTR FAMILY 7.2)	Chr_07:20108624..20110840 reverse	-14.9934	0.019298
Minas.08G203500	XTH15 (xyloglucan endotransglucosylase/hydrolase 15)	Chr_08:20304998..20306275 reverse	-1.33469	0.020687
Minas.07G085900	AGD11 (ARF-GAP domain 11)	Chr_07:15845009..15846439 forward	-0.69172	0.021084
Minas.10G078500	PSE1 (PB-SENSITIVE1)	Chr_10:4070869..4073204 reverse	-8.74699	0.024442
Minas.03G040700	STZ (salt tolerance zinc finger)	Chr_03:15408894..15410016 forward	-2.61555	0.024442

Table 4. Continued.

Transcript ID	Araport11 Homolog	Physical Location	Log2 FC	P-value adj.
Minas.09G118500	EXO70D1 (exocyst subunit exo70 family protein D1)	Chr_09:26376388..26379039 reverse	-1.19867	0.024442
Minas.12G129600	CAX9 (cation exchanger 9)	Chr_12:18570776..18573367 reverse	-0.67925	0.024442
Minas.02G057500	EXL2 (EXORDIUM LIKE 2)	Chr_02:2745154..2746374 reverse	-0.64328	0.025701
Minas.14G049700	RLP2 (receptor like protein 2)	Chr_14:2606009..2608552 forward	-0.54371	0.028655
Minas.05G109800	AtMYB103 (myb domain protein 103), MYB103 (myb domain protein 103)	Chr_05:24164924..24167062 reverse	-14.2033	0.035319
Minas.12G166100	HSC70-1 (HEAT SHOCK COGNATE PROTEIN 70-1)	Chr_12:20180131..20183573 forward	-0.39417	0.037083
Minas.07G071200	HOG1 (HOMOLOGY-DEPENDENT GENE SILENCING 1)	Chr_07:5212530..5215870 reverse	-0.29842	0.038479
Minas.10G005000	EXPA8 (expansin A8)	Chr_10:191947..193408 forward	-0.44568	0.040224
Minas.11G045700	LRX4 (LEUCINE-RICH REPEAT EXTENSIN 4)	Chr_11:2138907..2142412 reverse	-0.54804	0.042626
Minas.14G303800	ERF110 (ETHYLENE RESPONSE FACTOR 110)	Chr_14:26082415..26083723 reverse	-13.9012	0.044682
Minas.05G086000	PLH2	Chr_05:19403066..19408318 reverse	-8.46516	0.045282

Population-Specific Gene Expression: A Comparison Between HHR and SHL

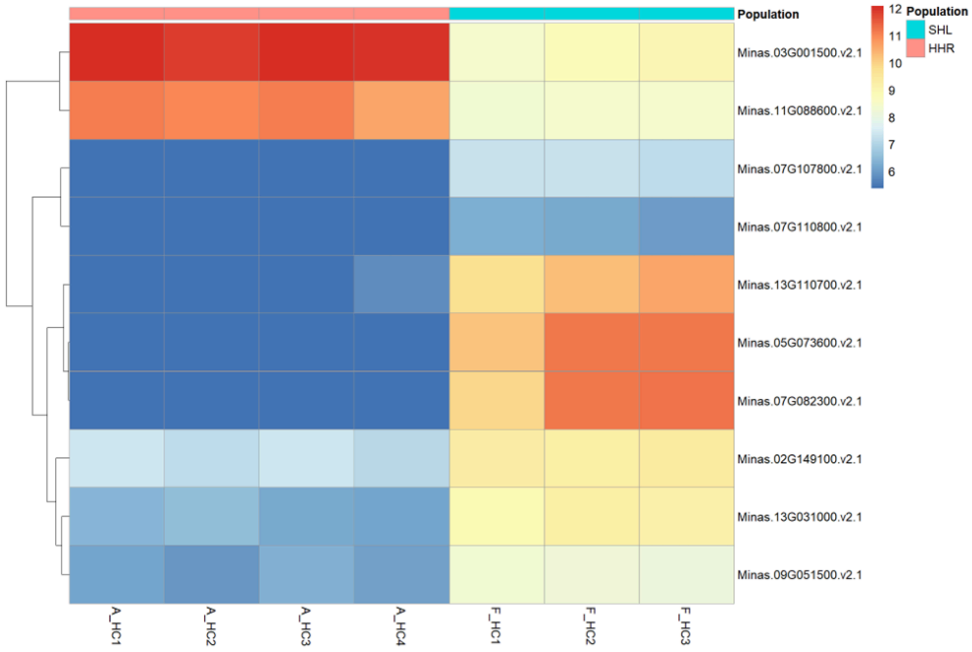

Figure 16. Heatmap showing variation in gene expression across the top 10 significantly differentially expressed genes between populations HHR and SHL in Model 2. Rows represent Transcript ID, and columns represent individual samples grouped by population. On the heat map, red indicates high values of gene expression while blue indicates low values of gene expression.

Table 5. Top 10 most significantly differentially expressed genes between populations HHR and SHL in Model 2. Transcript IDs represent the first isoform of each differentially expressed gene from the *Mimulus nasutus* annotation. The Arabidopsis homolog indicates the most similar (e-value) gene in *Arabidopsis thaliana*. Log_2 fold change reflects the magnitude of expression change in offspring, and adjusted p-values account for multiple testing ($\alpha = 0.05$).

Transcript ID	Araport11 Homolog	Physical Location	Log2 FC	P-value adj.
Minas.05G073600	CRK29 (CYSTEINE-RICH RLK (RECEPTOR-LIKE PROTEIN KINASE) 29)	Chr_05:5254767..5259260 forward	-37.2374	2.01E-73
Minas.07G110800	KUP3 (K+ UPTAKE TRANSPORTER 3)	Chr_07:23072311..23074340 forward	-27.8713	1.66E-47
Minas.07G107800	KUP3 (K+ UPTAKE TRANSPORTER 3)	Chr_07:19956522..19959649 forward	-28.089	2.86E-46

Table 5. Continued.

Transcript ID	Araport11 Homolog	Physical Location	Log2 FC	P-value adj.
Minas.03G001500	tetratricopeptide repeat (TPR)-containing protein	Chr_03:699346..710908 reverse	3.819879	9.45E-45
Minas.13G031000	Protein phosphatase 2C family protein	Chr_13:3192479..3196799 forward	-4.47253	8.19E-37
Minas.09G051500	F-box/RNI-like superfamily protein	Chr_09:20720178..20722514 reverse	-4.32291	2.37E-31
Minas.11G088600	DJ1D	Chr_11:15709962..15714192 forward	2.939513	7.25E-29
Minas.13G110700	alpha/beta-Hydrolases superfamily protein	Chr_13:20253897..20255357 forward	-9.79596	1.01E-28
Minas.02G149100	ARGAH1 (ARGININE AMIDOHYDROLASE 1)	Chr_02:19336142..19339420 forward	-2.84954	1.27E-26
Minas.07G082300	NB-ARC domain-containing disease resistance protein	Chr_07:14124555..14131093 forward	-12.9647	1.88E-26

A total of 13 genes were identified as significantly upregulated (Table 3), and 46 genes were significantly downregulated (Table 4), all of which were successfully matched to homologs in *Arabidopsis thaliana* using BLASTP. The $\log_2$ fold change for upregulated genes ranged from 0.183 to 18.573 (Table 3), while downregulated genes exhibited Log_2FC values between -0.217 and -29.364 (Table 4). Between both upregulated and downregulated genes, differentially expressed genes were distributed across all 14 chromosomes of the genome, suggesting a genome-wide transcriptional response to heat stress in the parental generation.

When comparing population HHR to SHL, the top 10 most significantly differentially expressed genes were considered. This analysis revealed that downregulation occurred more frequently in HHR relative to SHL, suggesting a population-specific transcriptional response

(Table 5). Notably, the magnitude of expression differences between the two populations was stark and consistent across replicates (Figure 16).

DISCUSSION

Although previous research has provided some insight into the induction and persistence of transgenerational plasticity (TGP) in response to various abiotic stressors, the genetic basis mediating this phenomenon and its contribution to evolution remain poorly characterized. To address this gap, we investigated the genetic architecture underlying TGP and within-generation plasticity (WGP) and phenotypic variation in response to temperature. By using a MAGIC line crossing scheme, we leverage increased genetic diversity and recombination to map quantitative trait loci (QTL) associated with plastic trait responses. We complemented these results with gene expression data from offspring whose parents experienced either heat stress (HC) or control (CC) conditions.

Although no QTL were explicitly associated with TGP, this absence may reflect a highly polygenic architecture beyond the resolution of our mapping approach, or suggest that transgenerational effects may be inherited primarily through epigenetic modifications rather than genetic variation. In contrast, we identified large-effect QTL associated with mean phenotypic variation in traits such as mean tube length, mean corolla width, and mean anthocyanin pigmentation, all under cold parental x cold offspring conditions. Moreover, parental heat stress tended to induce widespread downregulation of gene expression in offspring, and the magnitude and direction of these responses varied significantly among populations.

Explanations for Genetic Map Distortion

Across all contigs, our total genetic map length was several thousand cM longer than expected. For context, a recent study constructing a linkage map for *M. laciniatus* x *M. guttatus* F2 population spanned a total length of 1264.61 cM across 14 linkage groups (Ferris et al. 2017). Several factors may explain the observed inflation in our map.

One key issue is the difference in minor allele frequency (MAF) distributions between founders and MAGIC crosses. Founding individuals exhibited a substantially higher median MAF than MAGIC crosses. This discrepancy is likely driven by differences in sequencing depth as the founders were sequenced using whole-genome sequencing (WGS) at ~8x coverage, while MAGIC lines were sequenced via ddRAD-seq at ~2x coverage. To account for these technical differences, we adjusted our variant filtering parameters, increasing the MAF from 0.05 to 0.15 and applying both minimum and maximum depth-of-coverage (DP) filters during variant-level filtration. However, despite these efforts, the founder MAF remained consistently higher than those in the offspring. These persistent differences suggest that applying uniform DP filters genome-wide may not be sufficient. Instead, it may be necessary to identify and exclude regions with very consistent high coverage in founders but little to no coverage in the MAGIC crosses. Focusing on genomic regions that are reliably covered in both sequencing types would help improve map quality by removing artifacts from further analysis.

Another challenge in constructing a reliable genetic map was the limited functionality of the R/qtl2 package. R/qtl2 is a widely used tool for QTL mapping and, unlike its predecessor R/qtl, supports multi-parental populations and high-dimensional data. However, its primary function for genetic map estimation, est_map(), is restricted to re-estimating inter-marker distance. It enforces stringent data formatting, requiring that markers remain within the same chromosome groups and maintain their original order as in the physical map. In other words, the package does not support *de novo* linkage group formation or marker reordering, which means the resulting genetic map may not accurately reflect the true order of inheritance. As a result, markers that are inherited together may appear artificially far apart in the genetic map.

Undetected QTL for TGP Responses?

The absence of detectable QTL for transgenerational plasticity (TGP) across all measured traits may reflect limited statistical power or the effects of noise, rather than a true lack of heritable genetic variation. This may be more likely if TGP has a highly polygenic genetic architecture characterized by many loci, each of small effect size.

Supporting this possibility, a recent study conducted on *Arabidopsis thaliana* (Che et al. 2024) identified multiple QTL for transgenerational phenotypic plasticity in response to variable light intensity, mapping 50 QTLs across 4 chromosomes for high-light intensity TGP and 34 QTLs across 3 chromosomes for low-light intensity TGP, with no overlap between the sets. Although they identified statistically significant loci, the large number and genomic distribution of these loci imply that TGP in *Arabidopsis* is context-dependent and highly polygenic. Similarly, this pattern was observed for within-generation plasticity in another study on *A. thaliana* (Zan and Carlborg 2019) found that within-generation plasticity for flowering time was associated with 48 different loci across multiple growth temperatures, further supporting the hypothesis that plastic responses are controlled by polygenic architecture.

In contrast, our study detected no QTL surpassing the 1000x permutation LOD threshold for TGP. Without increased statistical power, it is not possible to determine whether these traits could be explained by many small-effect loci. Our results could be confounded by genotypic noise or the sparsity of TGP values. For instance, calculating each TGP value required complete trait measurements across all four parental x offspring environmental combinations (HH, HC, CC, CH), and if a single value was missing for any genotype, the corresponding TGP value was omitted entirely. This effectively reduced our sample size by ~15% and, in turn, may have limited our ability to detect QTL of small effect in TGP.

Mean Floral Trait Variation in Cold Environments

Out of all measured traits, quantitative trait loci (QTL) were only detected for a subset of floral traits: corolla width, tube length, and anthocyanin pigmentation. Floral traits are known to exhibit substantial intraspecific variation, are typically heritable (Hansen et al. 2003), making them ideal candidates for investigating local adaptation.

Importantly, these QTL were only detected in environments in which both the parental and offspring generations experienced cold stress. This pattern indicates that the correlation between genotype and phenotypic variation is contingent upon a shared cold environment in both parental and offspring generations, suggesting that reliable parental cues are necessary to express phenotypic variation in floral traits.

Founder allelic effect sizes varied within these QTL, suggesting that populations differ in their genetic contributions to cold-responsive floral variation. This variation may reflect locally adapted phenotypic variation, where genotypes from certain populations are more responsive to parental cues than others. An elevational gradient in founder effect sizes is most apparent in the phenotypic variation of mean tube length: populations from low-to-mid elevations (e.g., SNB, HHR, and TRT) contribute positively to trait values, whereas populations from mid-to-high elevations (e.g., OPN, SHL, and PET) contribute negatively. This directional pattern suggests that floral tube length plasticity in response to cold x cold exposure may be shaped by elevation-specific environmental pressures, and is thus involved in local adaptation within M. laciniatus. These findings are congruent with previous studies on *M. laciniatus,* which have also found patterns of genetic variation in the mean phenotypic expression of mating system traits like corolla width and length, which were associated with elevation (Ferris and Syrotchen 2024).

QTL detection for flower anthocyanin is likely because cold temperatures are known to trigger the overproduction of reactive oxygen species (ROS), which contribute to a plant's oxidative stress. To counter this oxidative stress, plants can activate antioxidant pathways, including the synthesis of anthocyanins, which act as free radical scavengers by neutralizing ROS (Li and Ahammed 2023). The strong positive founder effects from HHR and TRT suggest that these populations may rely on increased anthocyanin production or buffer against oxidative stress endured during cold exposure.

One hypothesis for the QTL detected in corolla width under cold conditions is that it may result from pleiotropy, where the same genetic region influences both corolla width and WGP (Cold) mean flower anthocyanin. Given that both of these traits map to nearly identical QTL intervals on contig 11 (Table 2), this suggests that selection for increased anthocyanin production under cold stress may indirectly drive changes in floral morphology, such as reduced corolla width. In this scenario, floral size itself may not be under direct selection, but rather a correlated response to selection on anthocyanin production. However, further joint mapping efforts using a more accurate and reliable linkage map are necessary to confirm this relationship.

Heat Exposure Induces Differential Gene Expression in the Offspring Generation

Although we did not detect regions of the genome significantly correlated with transgenerational plasticity (TGP), we found that exposure to heat stress in the parental generation had a significant effect on gene expression in the offspring generation. These findings are consistent with our hypothesis that TGP may be inherited through pre-transcriptional modifications. We find evidence that differential gene expression acts

Downregulated genes

One gene found to be significantly downregulated, with a log2 fold change of -0.29842 (Table 4), was HOMOLOGY-DEPENDENT GENE SILENCING 1 (*HOG1*). *HOG1* encodes S-adenosyl-L-homocysteine hydrolase (SAHH), an enzyme that catalyzes the conversion of S-adenosyl-homocysteine (SAH) to homocysteine (Hcy). This reaction is critical, as SAH is a strong competitive inhibitor of S-adenosylmethionine (SAM), which serves as a methyl group donor (De La Haba and Cantoni 1959). Given that SAM acts as the primary methyl donor in many biological methylation reactions, including DNA methylation, the downregulation of *HOG1* likely leads to the accumulation of SAH, in turn competitively inhibiting SAM-dependent methylation. This downregulation may generally reduce methylation levels across the genome, particularly in stress-responsive regions. However, further research is needed to determine which genes or genomic regions are specifically impacted by downregulation of *HOG1*.

Another gene found to be significantly downregulated, with a log2 fold change of -15.0291 (Table 4), was C-REPEAT/DRE BINDING FACTOR 2 (*CBF2*). *CBF2* is a dehydration-responsive element-binding factor known to bind specifically to cold- and dehydration-responsive elements (Shinozaki 1994), promoting the transcription of downstream genes involved in freezing tolerance. The substantial downregulation of *CBF2* following heat stress in the parental generation suggests a transgenerational trade-off, where regulatory pathways involved with cold stress responses are suppressed following exposure to extreme heat.

We also observed significant downregulation of *WRKY41*, with a log2 fold change of -1.31743 (Table 4). WRKY is known to bind directly to the promoters of CBF genes (including CBF2), acting as a repressor (Wang et al. 2023). Given its repressive role, the downregulation of *WRKY41* should, in theory, result in increased *CBF2* expression. However, the simultaneous

downregulation of *WRKY41* and *CBF2* suggests a more complicated regulatory network. A likely explanation for this observation is that an alternative repressor suppresses the expression of *CBF2*.

Upregulated genes

One gene significantly upregulated in response to heat stress during the parental generation was *SPT16* (Suppressor of TY16), with a log2 fold change of 15.12106 (Table 3). *SPT16* is one of two subunits that form the FACT (Facilitates Chromatin Transactions) complex, a histone chaperone known to be involved in the expression of genes encoding anthocyanin biosynthetic enzymes. A recent study in *Arabidopsis thaliana* demonstrated that both subunits of the FACT complex, *SPT16* and *SSRP1*, are involved in the production of anthocyanin biosynthetic enzymes under moderate high-light stress (Pfab et al. 2018).

However, our results indicate that only *SPT16* is upregulated in response to heat stress during the parental generation. This finding suggests a potential imbalance in the expression of *SPT16* and *SSRP1* in the offspring generation, which could impair the formation of active FACT complexes. Such an imbalance could ultimately reduce the expression of anthocyanin biosynthesis genes in the offspring, reducing the plant's ability to be fully primed to combat reactive oxygen species (ROS) and oxidative stress. However, further investigation is required to determine whether the lack of SSRP1 upregulation in the parental generation directly leads to reduced *SSRP1* expression in the offspring generation or if differential regulation in *SSRP1* is lost by the offspring generation.

Another gene that was found to be significantly upregulated in response to heat stress in the parental generation was *PMEAMT* (phosphoethanolamine N-methyltransferase), with a log2 fold change of 15.9914 (Table 3). In *Arabidopsis thaliana*, *PMEAMT* is involved in the second and third methylation steps of the phospho-base methylation pathway, specifically converting phosphomethylethanolamine (PMEA) to phosphodimethylethanolamine (PDEA), and subsequently to phosphocholine (PCho) (BeGora et al. 2010). PCho can then either serve as the head group to phosphatidylcholine (PC) synthesis via the Kennedy pathway, or it can be converted back to Cho through dephosphorylation (Chen et al. 2018). Phosphatidylcholine (PC) is a major component of membrane lipids, and in response to heat stress, plants are known to

increase the proportion of PC to maintain the structural integrity of the lipid bilayer (Higashi and Saito 2019). This suggests that in response to heat stress experienced by the parental generation, *PMEAMT*'s promoters or regulatory regions may undergo heritable epigenetic modifications. Such epigenetic changes could result in the upregulation of *PMEAMT*, meeting the increased demand for PCho necessary for PC synthesis. Although *cis*-elements in phosphoethanolamine N-methyltransferase (*PEAMT*)--an enzyme that functions in the same phospho-base methylation pathway--were found to be responsive to abiotic stress in maize (Niu et al. 2018), the regulatory response of *PMEAMT* in *Arabidopsis* remains largely uncharacterized. Therefore, future studies should focus on investigating the regulatory response of *PMEAMT* under heat stress and determining whether these regulatory changes involve heritable epigenetic modifications.

Also found to be significantly upregulated in response to heat stress were JUMONJI DOMAIN-CONTAINING PROTEIN (*JMJ31*) proteins at a lesser magnitude of 0.235715 (Table 3). In brief, JMJ (JMJ30, JMJ32) proteins are histone demethylases that remove methyl groups from lysine residues on histones, typically resulting in the removal of repressive marks (e.g., H3K27me3, H3K3me2), poisoning genes for subsequent activation. However, the function of *JMJ31* remains largely uncharacterized and is hypothesized to be enzymatically inactive because it lacks the conserved amino acids (Gan et al. 2014). Therefore, it is unlikely that *JMJ31* plays a large role in any transgenerational effects.

Broader Implications and Future Directions

Because this study was largely hypothesis-generating, future work should focus on functionally validating the genes implicated here in transgenerational plasticity (TGP). Although epigenetic modifications are thought to underlie TGP, this study did not include methylome sequencing of individuals exposed to extreme temperature regimes. Consequently, it is not possible to definitively determine whether differential methylation occurred. Future efforts should integrate methylome and transcriptome analyses to better elucidate the epigenetic mechanisms governing TGP.

In addition, transgenerational effects observed in this study were tested under controlled greenhouse conditions. To confirm the role of transgenerational plasticity in nature, future studies

should consider performing reciprocal transplant experiments, where offspring from parents exposed to hot and cold environments are grown at varying elevations.

Because it is uncertain whether wild plant populations will be able to successfully counter the effects of rapid climate change, understanding plants' responses to projected environmental conditions equips us with biological insights that could inform conservation efforts. Populations better fit to tolerate abiotic stressors, such as extreme heat, have a greater likelihood of survival under similar environmental regimes. Therefore, determining the molecular mechanisms and strategies different populations employ to cope with stress, as well as how these strategies vary among populations, can better inform conservation practices such as gene flow or translocation. Especially for self-pollinating species like *M. laciniatus*, where exchange of genetic information is limited, facilitating genetic exchange could significantly improve resilience to projected climate regimes.

ACKNOWLEDGEMENTS

This thesis would not have been possible without the immense support from the Blackman Lab. I extend my sincere gratitude to Dr. Benjamin Blackman, postdoctoral researchers Dr. Jesus-Martinez Gomez and Dr. Allie Gaudiner, and Dr. Ren Haam for their invaluable guidance. Your mentorship has provided me with countless opportunities to grow and challenge myself as a researcher and has truly fostered my love for science. I am indebted to Dr. Patina Mendez for her phenomenal teaching, feedback, and continued encouragement. I express my immense appreciation to both the Rausser College of Natural Resources and the Rose Hills Summer Fellowship for funding this research. This thesis is dedicated in loving memory of my stepfather, Cliff Bradley, and my great-grandmother, Gloria Lasky. You both brought an abundance of joy and light into my life. I miss you dearly.

REFERENCES

Agrawal, A. A., C. Laforsch, and R. Tollrian. 1999. Transgenerational induction of defences in animals and plants. Nature 401:60–63.

Alvarez, M., A. Bleich, and K. Donohue. 2020. Genotypic variation in the persistence of transgenerational responses to seasonal cues*. Evolution 74:2265–2280.

BeGora, M. D., M. J. R. Macleod, B. E. McCarry, P. S. Summers, and E. A. Weretilnyk. 2010. Identification of Phosphomethylethanolamine N-Methyltransferase from Arabidopsis and Its Role in Choline and Phospholipid Metabolism. Journal of Biological Chemistry 285:29147–29155.

Bell, A. M., and J. K. Hellmann. 2019. An Integrative Framework for Understanding the Mechanisms and Multigenerational Consequences of Transgenerational Plasticity. Annual Review of Ecology, Evolution, and Systematics 50:97–118.

Broman, K. W., D. M. Gatti, P. Simecek, N. A. Furlotte, P. Prins, Ś. Sen, B. S. Yandell, and G. A. Churchill. 2019. R/qtl2: Software for Mapping Quantitative Trait Loci with High-Dimensional Data and Multiparent Populations. Genetics 211:495–502.

Che, J., Y. Wang, A. Dong, Y. Cao, S. Wu, and R. Wu. 2024. A nested reciprocal experimental design to map the genetic architecture of transgenerational phenotypic plasticity. Horticulture Research 11:uhae172.

Chen, S., Y. Zhou, Y. Chen, and J. Gu. 2018. fastp: an ultra-fast all-in-one FASTQ preprocessor. Bioinformatics 34:i884–i890.

Chen, W., M. C. Taylor, R. A. Barrow, M. Croyal, and J. Masle. 2019. Loss of Phosphoethanolamine *N* -Methyltransferases Abolishes Phosphatidylcholine Synthesis and Is Lethal. Plant Physiology 179:124–142.

Colicchio, J. M., and J. Herman. 2020. Empirical patterns of environmental variation favor adaptive transgenerational plasticity. Ecology and Evolution 10:1648–1665.

Colicchio, J. M., F. Miura, J. K. Kelly, T. Ito, and L. C. Hileman. 2015a. DNA methylation and gene expression in Mimulus guttatus. BMC Genomics 16:507.

Colicchio, J. M., P. J. Monnahan, J. K. Kelly, and L. C. Hileman. 2015b. Gene expression plasticity resulting from parental leaf damage in *Mimulus guttatus* . New Phytologist 205:894–906.

Danecek, P., A. Auton, G. Abecasis, C. A. Albers, E. Banks, M. A. DePristo, R. E. Handsaker, G. Lunter, G. T. Marth, S. T. Sherry, G. McVean, R. Durbin, and 1000 Genomes Project Analysis Group. 2011. The variant call format and VCFtools. Bioinformatics 27:2156–2158.

De La Haba, G., and G. L. Cantoni. 1959. The Enzymatic Synthesis of

S-Adenosyl-l-homocysteine from Adenosine and Homocysteine. Journal of Biological Chemistry 234:603–608.

Dobin, A., C. A. Davis, F. Schlesinger, J. Drenkow, C. Zaleski, S. Jha, P. Batut, M. Chaisson, and T. R. Gingeras. 2013. STAR: ultrafast universal RNA-seq aligner. Bioinformatics 29:15–21.

Endelman, J. B., and C. Plomion. 2014. LPmerge: an R package for merging genetic maps by linear programming. Bioinformatics 30:1623–1624.

Gan, E.-S., Y. Xu, J.-Y. Wong, J. Geraldine Goh, B. Sun, W.-Y. Wee, J. Huang, and T. Ito. 2014. Jumonji demethylases moderate precocious flowering at elevated temperature via regulation of FLC in Arabidopsis. Nature Communications 5:5098.

Hansen, T. F., W. S. Armbruster, M. L. Carlson, and C. PÉlabon. 2003. Evolvability and genetic constraint in *Dalechampia* blossoms: Genetic correlations and conditional evolvability. Journal of Experimental Zoology Part B: Molecular and Developmental Evolution 296B:23–39.

Higashi, Y., and K. Saito. 2019. Lipidomic studies of membrane glycerolipids in plant leaves under heat stress. Progress in Lipid Research 75:100990.

Huang, X., M.-J. Paulo, M. Boer, S. Effgen, P. Keizer, M. Koornneef, and F. A. Van Eeuwijk. 2011. Analysis of natural allelic variation in *Arabidopsis* using a multiparent recombinant inbred line population. Proceedings of the National Academy of Sciences 108:4488–4493.

Kelly, A. J., and J. H. Willis. 1998. Polymorphic microsatellite loci in *Mimulus guttatus* and related species. Molecular Ecology 7:769–774.

Lachmann, M., and E. Jablonka. 1996. The Inheritance of Phenotypes: an Adaptation to Fluctuating Environments. Journal of Theoretical Biology 181:1–9.

Li, H. 2013, May 26. Aligning sequence reads, clone sequences and assembly contigs with BWA-MEM. arXiv.

Li, Z., and G. J. Ahammed. 2023. Plant stress response and adaptation via anthocyanins: A review. Plant Stress 10:100230.

Love, J. M., and K. G. Ferris. 2024. Local adaptation to an altitudinal gradient: The interplay between mean phenotypic trait variation and phenotypic plasticity in Mimulus laciniatus. Perspectives in Plant Ecology, Evolution and Systematics 63:125795.

Love, M. I., W. Huber, and S. Anders. 2014. Moderated estimation of fold change and dispersion

for RNA-seq data with DESeq2. Genome Biology 15:550.

McKenna, A., M. Hanna, E. Banks, A. Sivachenko, K. Cibulskis, A. Kernytsky, K. Garimella, D. Altshuler, S. Gabriel, M. Daly, and M. A. DePristo. 2010. The Genome Analysis Toolkit: A MapReduce framework for analyzing next-generation DNA sequencing data. Genome Research 20:1297–1303.

Munir, J., L. A. Dorn, K. Donohue, and J. Schmitt. 2001. The effect of maternal photoperiod on seasonal dormancy in *Arabidopsis thaliana* (Brassicaceae). American Journal of Botany 88:1240–1249.

Nicotra, A. B., O. K. Atkin, S. P. Bonser, A. M. Davidson, E. J. Finnegan, U. Mathesius, P. Poot, M. D. Purugganan, C. L. Richards, F. Valladares, and M. Van Kleunen. 2010. Plant phenotypic plasticity in a changing climate. Trends in Plant Science 15:684–692.

Niu, G.-L., W. Gou, X.-L. Han, C. Qin, L.-X. Zhang, A. Abomohra, and M. Ashraf. 2018. Cloning and Functional Analysis of Phosphoethanolamine Methyltransferase Promoter from Maize (Zea mays L.). International Journal of Molecular Sciences 19:191.

Pfab, A., J. T. Grønlund, P. Holzinger, G. Längst, and K. D. Grasser. 2018. The Arabidopsis Histone Chaperone FACT: Role of the HMG-Box Domain of SSRP1. Journal of Molecular Biology 430:2747–2759.

Schlichting, C. D. 2024. The Evolution of Phenotypic Plasticity in Plants.

Syrotchen, J. M., and K. G. Ferris. 2024. Local adaptation to an altitudinal gradient: The interplay between mean phenotypic trait variation and phenotypic plasticity in *Mimulus laciniatus*. *bioRxiv*, 2023.08.02.551729. [Preprint].

Uller, T., S. Nakagawa, and S. English. 2013. Weak evidence for anticipatory parental effects in plants and animals. Journal of Evolutionary Biology 26:2161–2170.

Wang, H., Y. Chai, X. Chu, Y. Zhao, Y. Wu, J. Zhao, F. Ngezahayo, C. Xu, and B. Liu. 2009. Molecular characterization of a rice mutator-phenotype derived from an incompatible cross-pollination reveals transgenerational mobilization of multiple transposable elements and extensive epigenetic instability. BMC Plant Biology 9:63.

Wang, X., Z. Li, Y. Shi, Z. Liu, X. Zhang, Z. Gong, and S. Yang. 2023. Strigolactones promote plant freezing tolerance by releasing the WRKY41 ‐mediated inhibition of *CBF* / *DREB1* expression. The EMBO Journal 42:e112999.

Yamaguchi-Shinozakiaib, K., and K. Shinozaki. 1994. A Nove1 cis-Acting Element in an Arabidopsis Gene Is lnvolved in Responsiveness to Drought, Low-Temperature, or High-Salt Stress.

Zan, Y., and Ö. Carlborg. 2019. A Polygenic Genetic Architecture of Flowering Time in the Worldwide *Arabidopsis thaliana* Population. Molecular Biology and Evolution 36:141–154.

APPENDIX

Figure A1. Linear regression of genetic position (cM) as a function of physical position (bp) across all contigs for three mapping populations (Crosses A, C, and E). Each line represents the best-fit regression for a given cross, with red, green, and blue corresponding to Cross A, Cross C, and Cross E, respectively.

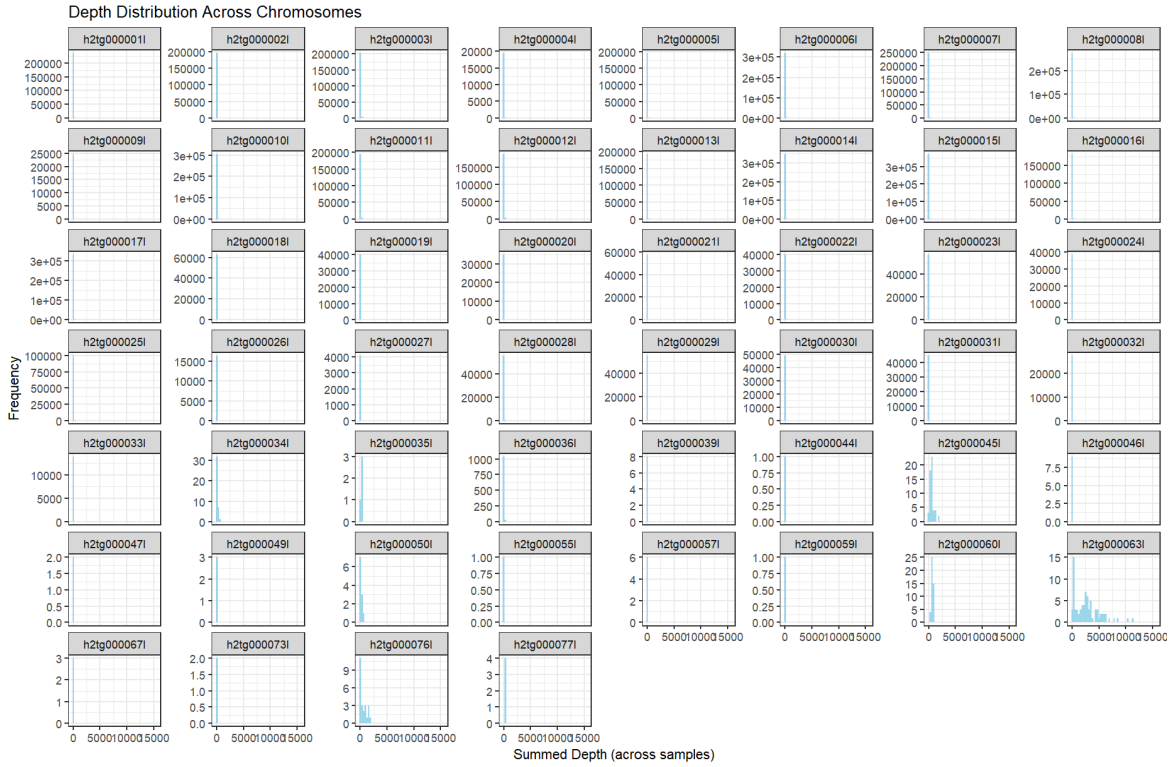

Figure A2. Histograms of summed site-level read depth (DP) across all contigs from the joint founder line VCF.